PERGAMON

International Journal of Heat and Mass Transfer 44 (2001) 3931–3940

International Journal of HEAT and MASS TRANSFER

www.elsevier.com/locate/ijhmt

Liquid blockage of vapor transport lines in low Bond number systems due to capillary-driven flows in condensed annular films

Jeffrey S. Allen [a,*], Kevin P. Hallinan [b]

[a] *National Center for Microgravity Research on Fluids and Combustion, NASA Glenn Research Center, Mail Stop 110-3, 21000 Brookpark Road, Cleveland, OH 44135, USA*

[b] *Department of Mechanical and Aerospace Engineering, University of Dayton, 300 College Park, Dayton, OH 44169, USA*

Received 5 October 1999; received in revised form 20 December 2000

Abstract

An experimental capillary-pumped loop (CPL) was designed to investigate the behavior of phase-change heat transfer devices and ascertain the mechanisms which have caused anomalous behavior of previous CPL demonstrations in low gravity. Low-gravity experiments were conducted during the Microgravity Science Laboratory (MSL-1) mission on-board the Space Shuttle Columbia in July of 1997. An interesting phenomenon resulting from liquid flow in an annular film was observed while investigating operation of the experimental CPL in low gravity. To the authors' knowledge, observation of this phenomenon has not been previously reported. In every test run performed, liquid would accumulate in the curved portion of the vapor leg. The accumulation of liquid would continue until the liquid lobe would suddenly transition into a slug of liquid. The liquid slug would prevent the flow of vapor to the condenser; eventually resulting in dryout of the condenser. Since liquid was no longer fed to the evaporator from the condenser, the CPL would ultimately fail. Analysis reveals that the formation of the slug is a consequence of both capillary pressure differences in the liquid film present in the curved section of the vapor leg and a long wavelength instability of the liquid film. This analysis also reveals the conditions under which the formation of such liquid slugs are inevitable.

1. Introduction

The utilization of space has become routine over the last several decades as evidenced by the large numbers of communication satellites, weather satellites, and manned missions that currently include the Space Shuttle, the Mir Space Station, and very soon the International Space Station. Issues such as power generation, orbit control, communications, and life support systems have had to be resolved to make space technology feasible. While certain technologies have matured, others have not. Thermal management is an area under extensive research because one of the many concerns when working in space is overheating of the spacecraft and spacecraft systems.

Single-phase heat transfer systems have been used for the purpose of transferring heat from the spacecraft interior. But these systems, while thermally effective, are inefficient and large. Another concern with single-phase systems is their reliance upon a mechanical pump to circulate the fluid. In addition to being a source of vibrations on board the spacecraft, a mechanical pump generates heat and requires a significant amount of energy in an environment where energy is at a premium. Also, the problems associated with replacing a defective pump in space can be enormous; especially if the liquid is hazardous. Therefore, an alternative heat transfer system has been sought.

One alternative device that has received considerable attention in the last decade is the capillary-pumped loop

* Corresponding author. Tel.: +1-216-433-3087; fax: +1-216-433-3793.

E-mail addresses: jeff.allen@grc.nasa.gov (J.S. Allen), kevin.hallinan@udayton.edu (K.P. Hallinan).

0017-9310/01/$ - see front matter
PII: S0017-9310(01)00036-9

Nomenclature

English symbols

a	acceleration
h	annular film thickness
L	characteristic length scale
P	pressure
r	radial dimension
R_b	radius of bend
R_i	inside radius of tube
t_λ	long wavelength instability timescale
t_σ	capillary-driven flow timescale
$t^*_{\lambda\sigma}$	dimensionless timescale
u	radial velocity
U	radial velocity scale
v	azimuthal velocity
V	azimuthal velocity scale

Greek symbols

δ	dimensionless film thickness
Γ	radii ratio
λ_D	wavelength
μ	absolute viscosity
ρ	liquid density
σ	surface tension
τ_s	surface shear stress

Dimensionless groups

Bo	Bond number, $\rho a L^2/\sigma$
Ca	Capillary number, $\mu U/\sigma$
Oh	Ohnesorge number, $\mu/\sqrt{\rho\sigma L}$
Re	Reynolds number, $\mu UL/\rho$

Subscripts

v	vapor phase
l	liquid phase
1	region 1 of liquid film
2	region 2 of liquid film
3	region 3 of liquid film
4	region 4 of liquid film

Superscripts

*	dimensionless variable

Units

cm	10^{-2} meters
mm	10^{-3} meters
μm	10^{-6} meters
s	seconds

(CPL); first developed at the NASA John H. Glenn Research Center at Lewis Field [1] in Cleveland, Ohio [1]. The basic operation of a capillary-pumped loop (CPL) is illustrated in Fig. 1. Heat is added to a porous wick, shown on the left side of the loop, causing the liquid to evaporate. In theory, the evaporation results in a slightly higher pressure at the wick which forces the vapor over to the cold side of the loop. There the liquid recondenses and is then pulled back to the evaporator by the capillary pressure difference between the condenser meniscus and the menisci in the evaporator wick. The pumping potential of a wick is not great. But since there is little resistance to liquid flow, the liquid can be moved over very long distances with relative ease. Some capillary-pumped loops tested on the ground have transferred heat over 20 m [1].

The promise of CPL's in space applications arises from the tremendous heat transport capability of these capillary-driven devices. These devices are much more efficient in the transfer of thermal energy than single-phase systems and, therefore, can be built much smaller and lighter. In addition, these capillary-driven devices require no power, generate no additional heat, and produce no vibrations.

Space-based demonstrations of CPLs have, at times, behaved unexpectedly. Pressure oscillations would arise, particularly at low heat fluxes and at startup. While the effect of the pressure oscillations could be modeled, the physical mechanism generating the pressure perturbations could not be explained. [2–6] The experiment described herein was designed to test the hypothesis that one source of pressure perturbations was due to destabilization of the evaporating menisci in the CPL wick.

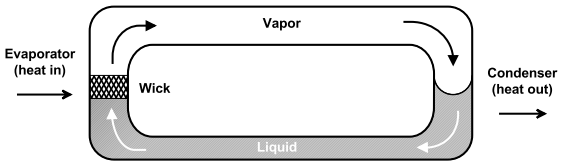

Fig. 1. Idealized operation of a CPL.

2. Experiment

The experiment, known as the capillary-driven heat transfer (CHT) experiment, was designed and developed for flight on the Space Shuttle Columbia during the first Microgravity Science Mission (MSL-1) in July 1997. An idealized glass CPL was constructed in order to observe the behavior of an evaporating meniscus within a closed phase-change heat transfer loop.

[1] Previously known as the NASA Lewis Research Center.

The principle component of the CHT experiment was an instrumented glass test loop which is illustrated in Fig. 2. Details of the rationale for the design of the experiment are described elsewhere [7]. A three-way valve, referred to as the control valve, directed liquid flow from the reservoir into the condenser leg and/or the evaporator leg of the test loop. During the experiment, the control valve allowed for liquid flow from the condenser leg to the evaporator leg while isolating the reservoir. The reservoir was constructed from a 10 cc gas tight syringe with a screw type plunger which allowed for repeatable fills. The liquid leg of the test loop was constructed from a Pyrex capillary with an inside diameter of 1 mm. The vapor leg of the test loop was constructed from 10 mm inside diameter Pyrex tube. Two conical transition sections connected the vapor leg to the liquid leg. The conical sections were designed to be capillary traps in low gravity so as to preferentially locate the evaporator meniscus. A capillary pumping potential was established by the difference between the pressure drop across the condenser meniscus in the 10 mm diameter tube and the pressure drop across the evaporator meniscus in the 1 mm diameter capillary tube. The difference in the condenser and evaporator diameters allowed for the capillary pumping potential to be maintained even with a large temperature difference between the evaporator and condenser. For these experiments, the test fluid was spectroscopic grade ethanol which perfectly wetted the test loop. Heat was applied to the evaporator by either of two resistance heaters attached to the capillary tube. Cooling of the condenser meniscus was accomplished by forced air convection at ambient temperature. Instrumentation included 7 thermocouples along the length of the evaporator leg and 4 thermocouples along the length of the condenser leg. An additional thermocouple and a pressure transducer were connected to the vapor leg. The position and behavior of both the condenser meniscus and the evaporator meniscus were recorded using a single video camera.

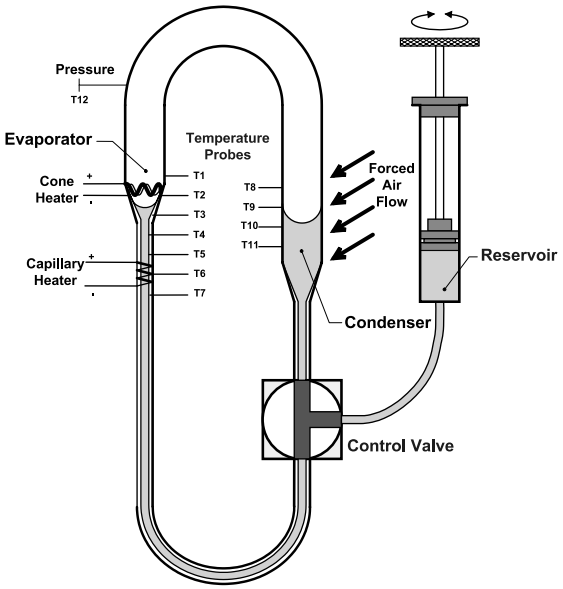

Fig. 2. Schematic of CHT experiment test cell.

3. Experimental observations

One of the first experimental observations, irrespective of the gravitational environment, was the formation of a continuous liquid film over the entire length of the vapor leg. Immediately after applying heat, a liquid film could be seen advancing up the wall of the vapor leg. This, in and of itself, is not a surprising result. Just beyond the evaporator meniscus the vapor is superheated relative to the test loop surface and it is expected that the vapor would condense immediately. Also, because ethanol perfectly wets the glass surface, the condensing vapor should form a liquid film as opposed to droplets. In normal gravity, the liquid film drains into both the condenser meniscus and into the evaporator cone section. The latter film drainage affected the stability of the evaporating meniscus by introducing cold fluid into localized areas of the meniscus. In low gravity, the liquid film also drains, but the draining occurs as a result of capillary forces.

Capillary forces "drain" the liquid film in the curved sections of the vapor leg. During each experiment run, the liquid accumulated in the outer portion of the curve in the vapor leg of the test loop. This pool of liquid would collect into a lobe which would grow until a slug of liquid would form, completely bridging the vapor line. Fig. 3 shows the formation of the liquid slug in the vapor leg during one of the low-gravity experiments. Viewing the sequence of images from left to right in Fig. 3, the liquid film begins to pool in the outer radius of the bend region eventually bridging. Prior to complete bridging of the vapor line, there is no observed adverse effect on the CPL operation due to the pooling of the liquid in the bend of the vapor leg. However, after the liquid slug forms, condensation at the condenser meniscus is greatly reduced. Subsequently, as liquid is continually fed to the evaporator, the condenser meniscus begins to recede. Eventually, the condenser meniscus recedes into the capillary tube thereby eliminating the pressure difference feeding liquid into the evaporator. At this point the evaporator deprimes and the system fails.

4. Annular liquid films

The condensation of the vapor on the inside of the loop results in the continuous annular liquid film. In a

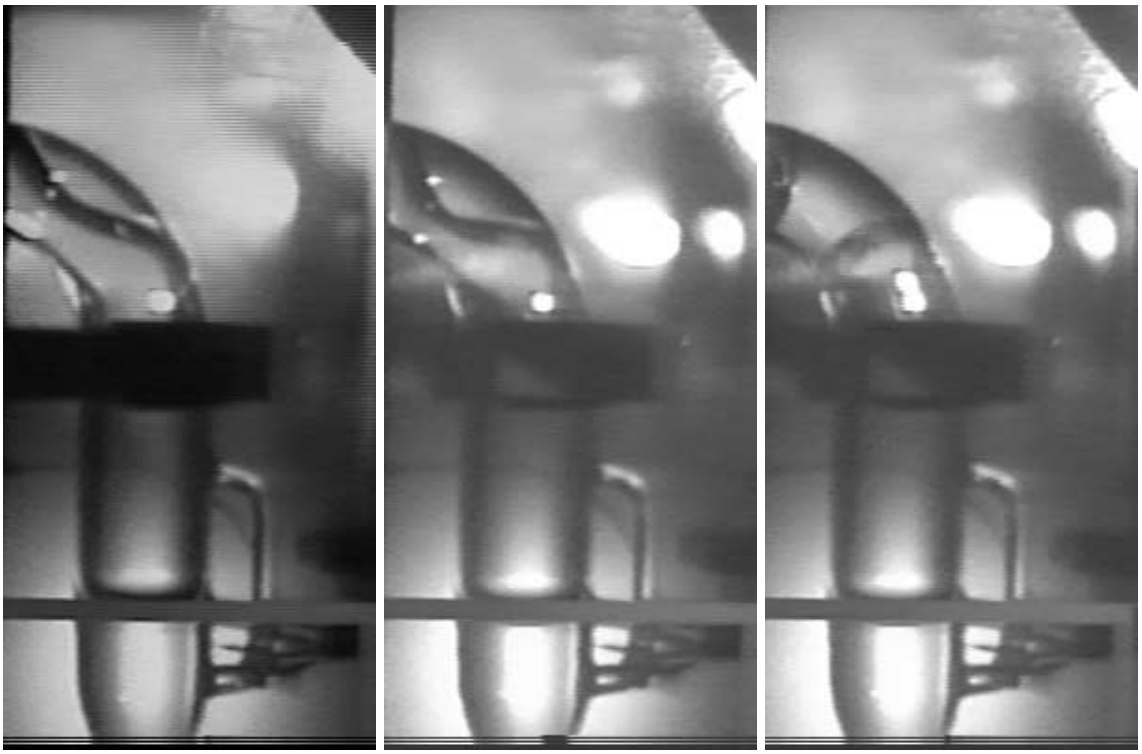

Fig. 3. Formation of a liquid slug in the bend of the vapor leg.

horizontal condenser under normal-gravity conditions without a large vapor flow Reynolds number, the annular film will drain to form a stratified two-phase system. Under low-gravity conditions, however, the dynamics of the annular film are governed by a balance between capillary forces and shear forces at the liquid–vapor interface.

It has long been recognized that an annular liquid film is unstable to long wavelength instabilities [8–15]. For annular films without an imposed axial flow and no surface shear, it has been observed that the liquid will accumulate into lobes and, if the volume of liquid is sufficient, into lenticular lenses which "pinch-off" the core fluid. The formation of a lenticular lens from the liquid in the annular film is also referred to as "snap-off" of the core fluid. Whether the adjacent lobes/lenses are connected to one another by a liquid film depends upon the static contact angle between the liquid and the tube [16]. For the purposes of this paper, annular film breakup will refer to either the formation of lenticular lenses or the break up of the thin film connecting liquid lobes since both conditions represent a stable liquid configuration.

Goren [13], using a linear stability analysis, determined the wavelength which gives rise to the fastest growth of a perturbation for various film thicknesses and Ohnesorge number, *Oh*. The Ohnesorge number, $\mu/\sqrt{\rho\sigma R_i}$, is a ratio of viscous forces to surface tension and inertial forces. Hammond [14] extended Goren's linear analysis and examined the nonlinear growth rates using the thin film approximation ($h/R_i \ll 1$). Hammond determined the characteristic time for evolution of the interface to be

$$t_\lambda \sim \frac{\mu R_i^4}{\sigma h^3}, \tag{1}$$

where μ is the absolute viscosity of the liquid film and σ is the surface tension. The disturbance wavelength, λ_d, resulting in the fastest growth was found to be $2^{3/2}\pi R_i$.

Gauglitz and Radke [11] modified the nonlinear analysis of Hammond by using the small slope assumption in place of the thin film assumption. The critical film thickness required for lens formation was found to be $0.12R_i$ and the experimentally determined critical film thickness was found to be $0.09R_i$. The initial growth rate was found to be exponential, but quickly slowed to the growth rate calculated in the linear stability analysis. As the lobe neared lens formation size, the growth rate rapidly increased due to non-linear effects. However, the initial and final growth times of the liquid film disturbance are insignificant relative to the slow growth period. The characteristic time of the slow growth period is the same as that expressed in Eq. (1).

Everett and Haynes [10], in a study of condensation in capillary tubes, examined the surface energy of constant curvature interfaces. They report that as the liquid film forms a lobe of critical volume, the surface energy can be minimized by reorienting the liquid lobe into a lenticular lens. Though the quasi-equilibrium analysis does not give information on the rate of this reorientation, the energy jump associated with the reorientation can be significant indicating a relatively rapid process.

The lobe formation and film breakup/lens formation has also been studied in the presence of an imposed axial flow. In most instances, these studies were conducted by displacing liquid in a capillary with an elongated gas bubble. In one such study [12], the liquid film surrounding the gas bubble in the flat film region did not have any apparent motion and the disturbance wavelength and growth rates were consistent with the linear stability analysis of Goren. Aul and Olbricht [17] studied lobe formation in flowing liquid films at low Reynolds numbers and found that the wavelength of the most unstable disturbance is independent of the Reynolds number for $Re < 100$. Interestingly, the liquid lobes were relatively stationary compared to the velocities in the liquid film and the core. For core flow velocities of 480 μm/s, the lobe velocity was less than 0.1 μm/s. After the liquid lobe had transformed into a lenticular lens, the lens acquired a velocity equal to that of the core (480 μm/s). The authors also report that the imposed flow enhanced the liquid transport into a particular lobe at the expense of its neighbor.

Many studies have been conducted on the destabilization of a liquid film due to interfacial shear. Hickox [18] examined instabilities on an annular film resulting from the difference in viscosity at the fluid–fluid interface. At very small Reynolds numbers, the interface destabilized due to capillary effects and at high Reynolds numbers the interface destabilized due to shear effects. Under certain conditions, axisymmetric disturbances were found to be stabilized, but no conditions existed for which the primary flow was stable to both axisymmetric and asymmetric disturbances.

Frenkel et al. [19] examined those conditions under which core flows could stabilize capillary instabilities on an annular film. Using a linear stability analysis with the thin film approximation, the determined a growth rate of the capillary instability which is consistent with Eq. (1). A non-linear analysis resulted in the same characteristic time scale. They found that the annular film did not break up over a small range of Capillary numbers, Ca, and Reynolds numbers, Re. The analysis of Frenkel et al. [19] is applicable when the Capillary number, $Ca \gg \delta^3$ and $Re \ll 1/\delta$, where δ is a dimensionless film thickness and the parameters Ca and Re are based on the interfacial velocity. These limits imply that the annular film must be very thin in order to be shear stabilized. In addition, the viscosity of the film was the same as the viscosity of the core in this analysis. Therefore, though interfacial shear was shown to saturate symmetric capillary instabilities, instabilities induced by viscosity stratification were not addressed.

Hu and Joseph [20] performed a linear stability analysis of core-annular flow allowing viscosity and density to vary across fluid interfaces. Of particular interest for two-phase heat transfer systems is the result that when the more viscous fluid resided in the annular film, the interface is unstable at *all* Reynolds numbers. Hu and Joseph found that at the lowest Reynolds numbers the long wavelength instability was the dominant mechanism and at higher Reynolds numbers instabilities arose due to interfacial shear which is consistent with Hickox as well as Aul and Olbricht.

Film breakup also occurs as bubbles pass through orifices or constrictions in liquid filled capillary tubes. Arriola et al. [9] studied the pinch-off of a oil drops moving through water in a constricted, square capillary tubes. They report that the pinch-off of the oil drop occurs slightly upstream of the center of the orifice. Ransohoff et al. [21] considered the effect of liquid flow in corners on the snap-off of a gas bubble in constricted square capillaries. It was found that above a critical Capillary number, the characteristic time for snap-off was constant. Below the critical Capillary number, the time for snap-off was inversely proportional to the Capillary number. The effect of the thin film on the wall (not in the corner) was found to be of little impact on the time for snap-off. They also report that snap-off can only occur in the presence of a tube constriction which contrasts with in the study by Aul and Olbricht where snap-off was experimentally observed in square capillaries without any constriction.

Gauglitz and Radke [22] examined the breakup of the liquid film in constricted, cylindrical capillaries. The characteristic time for breakup was found to be consistent with Eq. (1). Under conditions related to the initial film thickness and the bubble velocity, two lobes were found to form; one on either side of the constriction and these lobes migrated towards the constriction due to differences in capillary pressure. The theory correlates Ca to pinch-off time and works relatively well for larger pores and for small pores with high Ca. The stability of liquid films in networks of small channels has also revealed capillary induced snap-off at channel constrictions and divergences [23–25].

The liquid accumulation and slug formation observed during the CHT experiment is similar to the pinch-off observed in constricted capillaries in that the phenomenon resulted from a combination of a long wavelength instability and capillary driven flow in the liquid film. It will be shown that when a capillary-dominated annular liquid film exists in a curved tube, the pressure in the liquid is not circumferentially uniform. The variation in pressure drives an azimuthal flow

which results in liquid accumulation in the low pressure region.

5. Capillary pressure analysis

Capillary effects are important whenever a liquid–vapor interface exists in a low Bond number environment. The Bond number, $Bo = \rho a R^2/\sigma$, is a ratio of gravitational acceleration effects to surface tension effects on a liquid–vapor interface; where ρ is the liquid density, a is the acceleration, R is the characteristic length scale, and σ is the surface tension. For a given liquid, the Bond number may be varied by changing either the gravitational acceleration or the characteristic length scale. A low-gravity environment naturally results in a small Bond number ($Bo \ll 1$). In the annular film studies described earlier, a small Bond number was obtained by using very small diameter channels and tubes.

In a low Bond number environment, an annular liquid film in a curved tube will flow from the inside radius of the curve to the outside radius of the curve because of the differences in liquid pressure between these two regions. This difference in liquid pressure occurs as a result of variations in curvature of the liquid surface within the curved tube. Careful distinction must be made between the radius of the tube and the curve (or bend) radius of the tube in order to avoid confusion during the discussion to follow. The tube radius is the inside radius of the tubing and will be designated as R_i. The bend radius of the tube is the radius of the tube as it curves around to form the test loop. The bend radius will be designated as R_b (see Fig. 4).

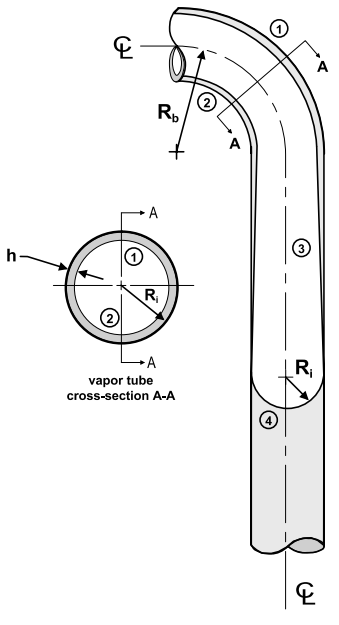

Fig. 4. Geometry of the annular liquid film illustrating the regions of interest.

The pressure and liquid flow within the bend are analyzed by examining four distinct regions of the annular liquid film as shown in Fig. 4. The first region is the outer portion of the tubing bend where the liquid accumulates. Region 2 is the inside radius of the tubing bend and is located 180° from region 1 at the same centerline location. Region 3 comprises the straight portion of the vapor line and region 4 is the condenser meniscus. Initially, the condenser meniscus is assumed to be relatively far from the bend. The liquid film flow will also be studied with the meniscus in the vicinity of the bend; i.e., when there is no region 3. For the purposes of this analysis the liquid film is assumed to be of uniform thickness, h.

The pressure drop across a liquid–vapor interface is known from the Laplace–Young equation:

$$P_v - P_l = \sigma\left(\frac{1}{R_1} + \frac{1}{R_2}\right), \tag{2}$$

where P_v is the vapor pressure, P_l is the liquid pressure, R_1 and R_2 are the principal radii of curvature, and σ is the surface tension. One of the principal radii of curvature is the same for each of the four regions and is equal to $R_i - h$. The second principal radius curvature varies from region to region. In region 1 that radius of curvature is $R_b + (R_i - h)$. Similarly, $-[R_b - (R_i - h)]$, ∞, and $R_i - h$ are the second principal radius of curvature for regions 2, 3, and 4, respectively. Table 1 lists the two principal radii of curvature for the four regions of interest as well as typical values of the principal radii of curvature for the CHT experiment.

In order to simplify the analysis, a film thickness ratio and a radii ratio are defined as

$$\delta \equiv \frac{h}{R_i} \quad \text{and} \quad \Gamma \equiv \frac{(R_i - h)}{R_b}. \tag{3}$$

Substituting the appropriate principal radii of curvature and the two ratios into the Laplace–Young equation results in a set of expressions for the pressure drop across the liquid surface for each of the four identified regions of the liquid film. For an isothermal system there will be no vapor flow between regions 1 and 2. Similarly, for an isothermal system without significant vapor flow, the pressure drop in the vapor between each of the other regions will be negligible. This assumption would have to be revisited when considering a system with a condensing vapor. Neglecting pressure variations in the vapor, the pressure drop across the liquid surface in each region as described by Eq. (2) can be rewritten so as to express the pressure drop within the annular liquid film between the various regions.

Table 1
Principal radii of curvature for the four regions of interest in the annular liquid film[a]

Region	Principal radii curvature		Typical values for CHT experiment	
	R_1	R_2	R_1 (mm)	R_2 (mm)
1	$R_i - h$	$R_b + (R_i - h)$	4.65	19.65
2	$R_i - h$	$-[R_b - (R_i - h)]$	4.65	−10.35
3	$R_i - h$	∞	4.65	∞
4	$R_i - h$	$R_i - h$	4.65	4.65

[a] The values for radii of curvature typical of the CHT experiment are based on a film thickness, h, of 350 μm, an inner tube radius, R_i, of 5 mm, and a bend radius, R_b, of 15 mm.

$$\Delta P_{l_{2-1}} = \frac{\sigma}{R_i(1-\delta)}\left[\frac{2\Gamma}{1-\Gamma^2}\right], \tag{4}$$

$$\Delta P_{l_{3-1}} = \frac{\sigma}{R_i(1-\delta)}\left[\frac{\Gamma}{1+\Gamma}\right], \tag{5}$$

$$\Delta P_{l_{2-3}} = \frac{\sigma}{R_i(1-\delta)}\left[\frac{\Gamma}{1-\Gamma}\right], \tag{6}$$

$$\Delta P_{l_{3-4}} = \frac{\sigma}{R_i(1-\delta)}. \tag{7}$$

Eqs. (4)–(7) describe the pressure difference within the annular liquid film when the condenser meniscus is relatively far from the tubing bend. If flow in the annular liquid film is assumed to be steady and dominated by viscous effects, then the governing equations can be reduced to the lubrication approximation. For $\delta \ll 1$ the velocity in the liquid film scales as:

$$U \sim \frac{(\delta R_i)^2}{\mu}\frac{\Delta P_l}{L} \tag{8}$$

where L is the length scale over which the pressure difference occurs. This scaling for U is only valid for values of $\Gamma \ll 1$. As Γ approaches 1, the bend radius approaches the inside radius of the tube. The curvature effects associated with R_b then become important and cannot be neglected. From region 2 to region 1 the appropriate length scale L, associated with the pressure difference, $\Delta P_{l_{2-1}}$, is πR_i. For the liquid flow between region 2 and region 3 and between region 1 and region 3 the length scale is the arc length from the bend to the straight section. The length scale used for the liquid flow near region 4 is half of the arc length of the meniscus.

The potential for liquid flow can be rewritten in terms of the Capillary number which scales the viscous forces against the capillary forces. Neglecting the aspect ratio of the annular liquid film, the Capillary number is defined as

$$Ca = \frac{\mu U}{\sigma}. \tag{9}$$

The appropriate Capillary numbers for flow between each of the four regions can be determined by combining the expressions for the pressure drop in the liquid film, ΔP_l, the length scale associated with the pressure drop, L, and the velocity scale in the liquid film, U. When the condenser meniscus is relatively far from the tubing bend, the resulting expressions for the Capillary numbers between each of the regions are shown in Eqs. (10)–(13).

$$Ca_{2-1} \sim \frac{2}{\pi}\left(\frac{\delta}{1-\delta}\right)^2\left[\frac{\Gamma}{1-\Gamma^2}\right], \tag{10}$$

$$Ca_{3-1} \sim \frac{2}{\pi}\left(\frac{\delta}{1-\delta}\right)^2\left[\frac{\Gamma}{1+\Gamma}\right]^2, \tag{11}$$

$$Ca_{2-3} \sim \frac{2}{\pi}\left(\frac{\delta}{1-\delta}\right)^2\left[\frac{\Gamma}{1-\Gamma}\right]^2, \tag{12}$$

$$Ca_{3-4} \sim \frac{2}{\pi}\left(\frac{\delta}{1-\delta}\right)^2. \tag{13}$$

The Capillary number development above applies when the meniscus is relatively far from the bend region; that is, when the distance is greater than $2\pi R_i$. When the meniscus is near the bend there is, in effect, no straight section (region 3) of the liquid film. For this case, the expressions for the Capillary numbers between the regions of the annular film are:

$$Ca_{2-1} \sim \frac{2}{\pi}\left(\frac{\delta}{1-\delta}\right)^2\left[\frac{\Gamma}{1-\Gamma^2}\right], \tag{14}$$

$$Ca_{1-4} \sim \frac{2}{\pi}\left(\frac{\delta}{1-\delta}\right)^2\left[\frac{1}{1+\Gamma}\right], \tag{15}$$

$$Ca_{2-4} \sim \frac{2}{\pi}\left(\frac{\delta}{1-\delta}\right)^2\left[\frac{1}{1-\Gamma}\right]. \tag{16}$$

During the CHT experiment, the thickness of the annular liquid film was estimated to be 350 μm. This estimate of the liquid film thickness is based on a uniform distribution of a volume of liquid over the entire surface of the vapor leg. The volume of liquid chosen was that which was lost from the condenser meniscus before the formation of the liquid slug. The inside radius of the vapor leg of the test loop is 5 mm and the bend radius of the test loop is 15 mm. Therefore, for the CHT experiment, the film thickness ratio, δ, is 0.07 and the radius ratio, Γ, is 0.31. Using these values for δ and Γ, the Capillary numbers present during the CHT experiment are calculated and shown in Table 2 for both the

Table 2
Typical Capillary numbers for the annular liquid film flow in the bend of the vapor leg during the CHT experiments

Meniscus far from bend ($>2\pi R_i$)		Meniscus near the bend ($<2\pi R_i$)	
Regions	$Ca \times 10^5$	Regions	$Ca \times 10^5$
2–1	124	2–1	124
3–1	20	1–4	275
2–3	73	2–4	523
3–4	361		

case where the condenser meniscus is relatively far from the tubing bend and for the case where the condenser meniscus is near the tubing bend.

The Capillary numbers for both positions of the condenser meniscus are represented pictorially in Fig. 5. Note that the starting and ending positions of the arrows is *not* intended to be indicative of transport distances. The arrows are only intended to indicate direction and relative magnitude of the flow in the annular liquid film. In Fig. 5(a), there is an azimuthal arrow representing $Ca_{2\text{–}1}$, a small arrow directed into the outer portion of the bend representing $Ca_{3\text{–}1}$, a second small arrow directed out of the inner portion of the bend representing $Ca_{2\text{–}3}$, and two large arrows directed into the meniscus representing $Ca_{3\text{–}4}$. Note that the $Ca_{3\text{–}4}$ arrows represent flow from the annular film in the straight section into the meniscus and do not represent flow from the bend into the meniscus. As reported by Aul and Olbricht [17], drainage by the meniscus will only occur over a length of $2\pi R_i$. If the distance between the meniscus and the bend is greater than $2\pi R_i$, the bend is effectively isolated from the meniscus. When the meniscus is relatively far from the tubing bend, liquid flow within the bend is much larger than the flow out of the bend and liquid will accumulate in the outer region (region 1) of the tubing bend. This result can be generalized to any low Bond number system and is not restricted to low-gravity systems. The liquid flow from region 3 into the condenser meniscus is higher than any other liquid film flows in the system. This implies that there is significant drainage into a meniscus even in low-gravity systems.

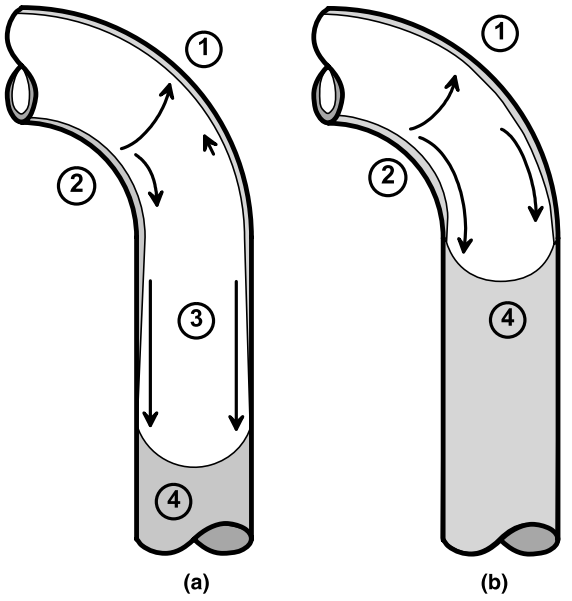

Fig. 5. Illustration of the direction and relative magnitude of liquid film flows for two cases; (a) the condenser meniscus relatively far from the tubing bend ($>2\pi R_i$) and (b) the condenser meniscus in the vicinity of the tubing bend ($<2\pi R_i$).

Similarly, for the case where the condenser meniscus is in the vicinity of the tubing bend; that is, less than $2\pi R_i$ from the bend (Fig. 5(b)), the liquid flow into the meniscus is an order of magnitude greater than any other liquid flow in the annular film. This has the effect of draining the bend region of the tube and can prevent the formation of the liquid slug *in that location only*. The formation of the liquid slug did appear to be inhibited during one run of the CHT experiment when the condenser meniscus was very near the bend; effectively draining the liquid out of the bend. However, condensation increased the thickness of the liquid film and as the condenser meniscus progressed away from the bend a liquid slug eventually did form.

The variation in the Capillary number between the various regions is a function of the geometry of the system and is not a function of the properties of the liquid (assuming constant temperature). Therefore, the liquid film flows illustrated in Fig. 5 are typical of the flows in any annular liquid film within a bend in a low Bond number system where the radii ratio, Γ, is between 0.1 and 0.4. As Γ decreases below 0.1, the liquid film flow characterized by $Ca_{2\text{–}1}$ is the dominant feature in the region of the bend, but is an order of magnitude less than the liquid flow into the condenser meniscus. At $\Gamma = 0.01$, $Ca_{2\text{–}1}$ will be two orders of magnitude less than the flow into the meniscus. Liquid film flows characterized by $Ca_{2\text{–}1}$ become significant relative to flows into the meniscus only when $\Gamma > 0.1$.

6. Characteristic time scales

The azimuthal flow described in Section 5 only occurs when there is a bend in the tubing. When $\delta \ll 1$, the film can be treated as planar and the characteristic flow time for the circumferential flow is $\mu_l R_b/\sigma\delta^2$. For thicker films, the radial dependence of the annular film must be retained. At times during the conduct of the CHT experiment, the estimate for δ was found to exceed 0.1.

The radial velocity component in the liquid film is represented by u and v is the azimuthal velocity component. U and V are the respective characteristic velocity scales. By non-dimensionalizing the radial dimension as $r = R_i(1 - \delta r^*)$, the annular liquid film thickness is scaled from 0 at the wall to 1 at the liquid-vapor interface. Applying these scales to the continuity equation results in $U/V \sim \delta$. Retaining only those terms of order δ or greater reduces the conservation of momentum equations to

$$\frac{\delta^2 R_i}{\mu_l V}\left(\frac{1}{1-\delta r^*}\right)\frac{\partial P}{\partial \theta} = \frac{\partial^2 v^*}{\partial r^{*2}} - \delta\left(\frac{1}{1-\delta r^*}\right)\frac{\partial v^*}{\partial r^*}. \tag{17}$$

Using the no-slip condition at the wall and the free shear condition at the liquid surface, the dimensionless velocity profile, v^*, can be expressed in terms of $O[\delta]$,

$$v^* = \frac{\delta^2 R_i \Delta P_\sigma}{\pi \mu_1 V}\left\{\left(r^* - \frac{1}{2}r^{*2}\right) + \delta\left(\frac{1}{2}r^{*2} - \frac{1}{3}r^{*3}\right) + \cdots\right\}, \tag{18}$$

where ΔP_σ is the capillary pressure drop within the liquid film.

At $r^* = 1, v^*$ is equal to 1 which results in a velocity scale of

$$V \sim \frac{\delta^2 R_i \Delta P_\sigma}{2\pi\mu_1}\left(1 + \frac{1}{3}\delta\right). \tag{19}$$

The characteristic time, t_σ, is found by dividing the distance of liquid flow, πR_i, by the velocity scale, V. Substituting the expression for the capillary pressure drop from region 2 to region 1, $\Delta P_{l_{2-1}}$, into the velocity scale, V, results in the following expression for the characteristic time of the capillary-driven flow:

$$t_\sigma \sim \frac{\pi^2 \mu_1 R_b}{\sigma \delta^2}\left(\frac{1-\Gamma^2}{1+(1/3)\delta}\right). \tag{20}$$

To reiterate, t_σ is the characteristic time for liquid to be convected 180° circumferentially within the bend.

These two time scales, Eqs. (1) and (20), characterize the rate of liquid accumulation in the vapor line. Liquid flow in the axial direction (scaled by t_λ) will always tend to form liquid lobes whenever the film length exceeds $2^{3/2}\pi R_i$. When there is a bend in the tube, azimuthal flow (scaled by t_σ) will result in liquid collecting in the outer portion of the tubing bend. The bend does not eliminate the long wavelength instability, but rather, the bend provides a perturbation to the liquid film which augments the long wavelength instability by locally increasing the liquid film thickness.

The importance of t_σ relative to t_λ can be examined by expressing the time scales as a ratio,

$$t^*_{\lambda_\sigma} = \frac{t_\lambda}{t_\sigma} \sim \frac{1}{\pi^2}\left[\frac{1+\delta/3}{\delta(1-\delta)}\right]\left(\frac{\Gamma}{1-\Gamma^2}\right). \tag{21}$$

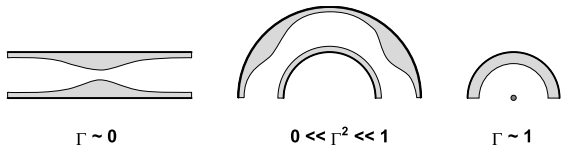

Fig. 6. Types of liquid accumulation in the bend of the vapor line for various values of Γ with $\delta < 0.1$. At $\Gamma \sim 0, t^*_{\lambda_\sigma} \sim 0$ and the liquid forms axisymmetric lobes. At $0 \ll \Gamma^2 \ll 1, t^*_{\lambda_\sigma} \sim 1$ and the liquid forms into non-axisymmetric lobes on the outer region of the bend. And at $\Gamma \sim 1, t^*_{\lambda_\sigma} \sim \infty$.

The ratio of tube radius to bend radius, Γ varies from a straight tube ($\Gamma = 0$) to a toroid with zero inside radius ($\Gamma = 1$). For straight tubing ($\Gamma = 0$), $t^*_{\lambda_\sigma} = 0$. This implies that $t_\sigma \sim \infty$ and that the film flow is only due to the long wavelength instability. The lobe formation will therefore be axisymmetric. When $\Gamma = 1$, the bend radius is equal to the tube radius; $R_b = R_i(1-\delta)$ and $t^*_{\lambda_\sigma} \to \infty$. For this case, $t_\sigma \ll t_\lambda$ and the liquid would accumulate uniformly in the outside radius of the tubing bend, but would not form lobes or slugs provided that $\delta \ll 1$. However, examining $t^*_{\lambda_\sigma}$ at $\Gamma \sim 1$ can be misleading since curvature effects of order δ^2 and higher may become important. For values of Γ^2 between 0 and 1, both flow mechanisms are important which results in non-axisymmetric lobe formation in the bend. In general, $t^*_{\lambda_\sigma}$ is approximately 1 when Γ is between 0.1 and 0.6, depending upon the value of δ. For the CHT experiments, $t^*_{\lambda_\sigma}$ is typically around 0.4. The effect of Γ on the liquid lobe formation is illustrated in Fig. 6.

The ratio $t^*_{\lambda_\sigma}$ is also a strong function of δ. The limits on $t^*_{\lambda_\sigma}$ can be expressed in terms of the relative values of Γ and δ. When $\delta \ll \Gamma \ll 1$, then $t^*_{\lambda_\sigma} \to \infty$ and the liquid film flow is characterized by t_λ. When $\Gamma \ll \delta \ll 1$, then $t^*_{\lambda_\sigma} \to 0$ and the liquid film flow is characterized by t_σ. The effect of very small film thicknesses on the characteristic flow times can be seen by examining Eqs. (1) and (20). The capillary time scale, t_σ, is proportional to δ^{-2} whereas the long wavelength instability timescale, t_λ, is proportional to δ^{-3}. Therefore, as the liquid film becomes very thin, t_λ increases more quickly than does t_σ.

7. Conclusions

During the operation of the CHT experiment both in normal gravity and in low gravity a liquid film formed over the entire vapor leg of the loop. In normal gravity, the draining of this film affected the stability of the evaporating meniscus, but was not directly responsible for evaporator dry out. In low gravity, however, the drainage of the annular liquid film resulted in an accumulation of liquid in the outer portion of the curve in the vapor leg. The liquid accumulation in this region bridged the vapor leg and blocked the flow of vapor to

the condenser meniscus. Subsequently, both condenser dryout and evaporator deprime ensued and the system failed. This mode of failure was not appreciated before the on-orbit experiment.

The CHT experiment has revealed a capillary flow phenomena which can result in an unexpected formation of a liquid slug. In any low Bond number system, an annular liquid film will flow circumferentially in a tubing bend as long as a continuous film exists because of capillary-driven flows. The conditions under which a non-axisymmetric liquid lobe will form out of the liquid collecting in the bend depend upon the geometry of the system, Γ, and the liquid film thickness, δ.

Acknowledgements

The authors' wish to thank the National Aeronautics and Space Administration (NASA) for supporting this research under grant number NAG3-191.

References

[1] F.J. Stenger, Experimental Feasibility Study of Water-Filled Capillary-Pumped Heat Transfer Loops, NASA TM X-1310, NASA Lewis Research Center, Cleveland, OH, 1966.

[2] D. Butler, Overview of CPL and LHP applications on NASA missions, in: AIP Conference Proceedings 458, in: Presented at the 1999 Space Technology and Applications International Forum (STAIF-99), Albuqurque, New Mexico, January 1999, pp. 792–798.

[3] D. Douglas, J. Ku, L. Schlager, Investigation of the starter pump purge superheat observed in the CAPL 1 Flight, AIAA 97-3871, in: 1997 National Heat Transfer Conference, Baltimore, Maryland, August 1997.

[4] K.R. Kolos, K.E. Herold, Low frequency temperature and fluid oscillations in capillary pumped loops, AIAA 97-3872, 1997 National Heat Transfer Conference, Baltimore, Maryland, 1997.

[5] J. Ku. Start-up issues in capillary pumped loops, in: Ninth International Heat Pipe Conference, Albuquerque, New Mexico, 1995.

[6] J. Ku, T. Hoang, An Experimental Study of Pressure Oscillation and Hydrodynamic Stability in a Capillary Pumped Loop, 1995 National Heat Transfer Conference, Portland, Oregon, 1995.

[7] J.S. Allen, Behavior of capillary-pumped loops in low gravity, Ph.D., University of Dayton, 1998.

[8] M. Abbasov, Z.M. Zorin, N.V. Churaev, Displacement of immiscible liquids in fine quartz capillaries. Displacement under the influence of a pressure differential, Kolloidnyi Zh. 51 (4) (1989) 634–639.

[9] A. Arriola, G.P. Willhite, D.W. Green, Trapping of oil drops in a noncircular pore throat and mobilization upon contact with a surfactant, Soc. Petrol. Eng. J. (February 1983) 99–114.

[10] D.H. Everett, J.M. Haynes, Model studies of capillary condensation. 1. Cylindrical pore model with zero contact angle, J. Colloid Interface Sci. 38 (1) (1972) 125–137.

[11] P.A. Gauglitz, C.J. Radke, An extended evolution equation for liquid film breakup in cylindrical capillaries, Chem. Eng. Sci. 43 (7) (1988) 1457–1465.

[12] H.L. Goldsmith, S.G. Mason, The flow of suspensions through tubes: II. Single large bubbles, J. Colloid Sci. 18 (1963) 237–261.

[13] S.L. Goren, The instability of an annular thread of fluid, J. Fluid Mech. 12 (1962) 309–319.

[14] P.S. Hammond, Nonlinear adjustment of a thin annular film of viscous fluid surrounding a thread of another within a circular cylindrical pipe, J. Fluid Mech. 137 (1983) 363–384.

[15] L.A. Newhouse, C. Pozrikidis, The capillary instability of annular layers and liquid threads, J. Fluid Mech. 242 (1992) 193–209.

[16] M.M. Weislogel, J.B. McQuillen, Hydrodynamic dryout in two-phase flows: Observations of low bond number systems. in: AIP Conference Proceedings 420, 1998 Space Technology and Applications International Forum (STAIF-98), Alburqurque, New Mexico, 25–29 January 1998, pp. 413–421.

[17] R.W. Aul, W.L. Olbricht, Stability of a thin annular film in pressure-driven, low-Reynolds-number flow through a capillary, J. Fluid Mech. 215 (1990) 585–599.

[18] C.E. Hickox, Instability due to viscosity and density stratification in axisymmetric pipe flow, Phys. Fluids 14 (2) (February 1971) 251–262.

[19] A.L. Frenkel, A.J. Babchin, B.G. Levich, T. Schlang, G.I. Sivashinsky, Annular flows can keep unstable films from breakup: nonlinear saturation of capillary instability, J. Colloid Interface Sci. 115 (1) (1987) 225–233.

[20] H.H. Hu, D.D. Joseph, Lubricated pipeling: stability of core-annular flow. Part 2, J. Fluid Mech. 205 (1989) 359–396.

[21] T.C. Ransohoff, P.A. Gauglitz, C.J. Radke, Snap-off of gas bubbles in smoothly constricted noncircular capillaries, AIChE J. 33 (5) (1987) 753–765.

[22] P.A. Gauglitz, C.J. Radke, The dynamics of liquid film breakup in constricted cylindrical containers, J. Colloid Interface Sci. 134 (1) (1990) 14–40.

[23] J.-D. Chen, Some mechanisms of immiscible fluid displacement in small networks, J. Colloid Interface Sci. 110 (2) (1986) 488–503.

[24] R. Lenormand, C. Zarcone, A. Sarr, Mechanisms of the displacement of one fluid by another in a network of capillary ducts, J. Fluid Mech. 135 (1983) 337–353.

[25] Y. Li, N.C. Wardlaw, Mechanisms of nonwetting phase trapping during imbibition at slow rates, J. Colloid Interface Sci. 109 (2) (1986) 473–486.